Investigation for antimagnetic rotational structure in ^{107,109,111}Pd*

Pooja Chauhan[1,2] Nithin V[1] Dalip Singh Verma[1†] S. Sihotra[2]

[1]Department of Physics and Astronomical Science, Central University of Himachal Pradesh, Dharamshala, District Kangra (H.P.)-176215 India
[2]Department of Physics, Panjab University, Chandigarh-160014, India

Abstract: Partial level schemes of ^{107,109,111}Pd have been reported in the literature, and antimagnetic rotational bands were recently predicted within the cranked shell model for the negative-parity bands of ^{107}Pd and ^{109}Pd, although lifetime data and semiclassical particle-rotor model studies are still unavailable. Electric quadrupole ($E2$) transitions have also been observed in the negative-parity band of ^{111}Pd, for which the rotational structure has not yet been theoretically investigated within the semiclassical particle-rotor framework. Over the past decade, the semiclassical particle-rotor model has been extensively applied to antimagnetic rotational bands in various nuclei, successfully explaining the generation of angular momentum through the shears mechanism and reproducing the observed systematics of excitation energies and $B(E2)$ transition rates. In the present work, the negative-parity bands of ^{107,109,111}Pd are investigated within the semiclassical particle-rotor model, where angular momentum is generated through the closing of proton-hole shears toward the neutron-particle angular momentum vector involving high-j orbitals. The calculated $B(E2)$ values decrease with increasing spin, while the ratio $\mathfrak{I}^{(2)}/B(E2)$ increases for the negative-parity bands of ^{107,109,111}Pd, consistent with the characteristic signatures of antimagnetic rotation.

Keywords: semiclassical particle-rotor model, antimagnetic rotation, palladium isotopes, high-spin states, $B(E2)$ transition rates, $\mathfrak{I}^{(2)}/B(E2)$ ratio

DOI: 10.1088/1674-1137/ae9f35 **CSTR:** 32044.14.ChinesePhysicsC.50114111

I. INTRODUCTION

In nuclei with proton numbers near shell closure, angular momentum is considered to be generated through the shears mechanism. It is described in terms of a single degree of freedom, known as the shear angle θ. The rotational mechanism includes both magnetic rotation (MR) [1, 2] and antimagnetic rotation (AMR) [3]. In the MR mechanism, angular momentum is generated through the simultaneous closing of the blades formed by valence neutrons and proton holes, whereas in the AMR mechanism, it is generated through the simultaneous closing of two proton-hole blades arranged symmetrically around the neutron-particle angular momentum vector (the twin-shears mechanism). In AMR, only $E2$ transitions are observed. This arises from the symmetric (two-shears) arrangement of the proton-hole blades, where the perpendicular components of their magnetic dipole moments cancel each other, leading to the absence of $M1$ transitions [4]. Antimagnetic rotation is a characteristic feature of nearly spherical or weakly deformed nuclei, where collective rotational motion is limited and angular momentum is generated through the symmetric closing of proton-hole shears. The Pd ($Z = 46$) isotopic chain, located near the $Z = 50$ shell closure and involving high-j proton ($g_{9/2}$) and neutron orbitals ($h_{11/2}$, $g_{7/2}$, $d_{5/2}$), provides a favourable configuration space in which antimagnetic rotational sequences may arise depending on the underlying particle-hole combinations.

Experimentally, AMR has been established through lifetime measurements in several nuclei, including the negative-parity band 2 of ^{100}Pd [5, 6], the negative-parity band 3 of ^{101}Pd [7, 8], the negative-parity band 1 of ^{103}Pd [9], the positive-parity band 2 of ^{104}Pd [10, 11], and the positive-parity bands 1 and 2 of ^{105}Pd [12], as well as in ^{105,106,107,108,109,110}Cd [13−19], ^{110}In [20], and ^{142,143}Eu [21, 22]. Theoretically, AMR has been successfully described within the semiclassical particle-rotor model for $^{105-111}$Cd [13, 15−17, 19, 23−26], ^{99,100,101,103,104,105}Pd [5, 6, 8−10, 27, 28], ^{127}Xe [29], ^{100,101,102}Ru [30−32], and ^{130}Ba [33, 34]. Within the cranked Nilsson-Strutinsky formalism, AMR has been described for ^{100}Pd [5]. The tilted ax-

Received 25 May 2026; Accepted 25 August 2026; Accepted manuscript online 26 August 2026

* The authors are grateful to the Central University of Himachal Pradesh and Panjab University, Chandigarh, for providing the necessary facilities to complete this work, as well as to the Department of Science and Technology, New Delhi, for the financial support provided to Prof. S. Sihotra under project DST(SERB-CRG/2022/000239)

† E-mail: dsverma@cuhimachal.ac.in (Corresponding author)

©2026 Chinese Physical Society and the Institute of High Energy Physics of the Chinese Academy of Sciences and the Institute of Modern Physics of the Chinese Academy of Sciences and IOP Publishing Ltd. All rights, including for text and data mining, AI training, and similar technologies, are reserved.

is cranking model has also been used to describe AMR in ^{58}Fe [35], ^{61}Ni [36], ^{101,102,103,104}Pd [37], ^{105,106,109}Cd [14, 23, 38], ^{108,109,110,112,113}In [20, 39–42], ^{130}Ba [33], ^{137,138}Nd [43–45], and ^{138}Sm [45, 46], while the cranked shell model (CSM) has been applied to ^{100,101,103,104,105,107,109}Pd [5, 47–50], ^{105,106,108}Cd [14, 15, 51], and ^{137,138}Nd [43, 44].

Partial level schemes for the Pd isotopes ^{107,109,111}Pd are available from heavy-ion fusion-evaporation experiments [52, 53], although experimental confirmation of AMR through lifetime measurements is lacking. AMR has been predicted only within the CSM for the negative-parity bands of ^{107,109}Pd, considering the configuration $\pi(g_{9/2})^{-4}\otimes\nu(h_{11/2})^3$ [49]. There has been neither theoretical nor experimental investigation of AMR in ^{111}Pd. These observations motivate the present investigation of the antimagnetic rotational structure in the negative-parity bands of ^{107,109,111}Pd using SCM.

In this work, the possibility of AMR in the negative-parity bands of ^{107,109,111}Pd has been investigated using SCM, in which the proton-hole and neutron-particle configuration has been optimised with respect to the experimental spin. The decreasing trend of the calculated electric quadrupole transition probability $B(E2)$ values and the increasing trend of the ratio $\Im^{(2)}/B(E2)$ are consistent with the characteristic signatures of AMR in the negative-parity bands of ^{107,109,111}Pd isotopes.

The paper is organised as follows: Section II explains the methodology used, the obtained results are discussed in Section III, and the conclusions of the work are presented in Section IV.

II. METHODOLOGY

In the semiclassical particle rotor model, a nucleus is regarded as a combination of a nuclear core and valence nucleons. The SCM describes the antimagnetic rotation mechanism by explaining how the experimentally observed total spin is generated in a weakly deformed nucleus through the geometric alignment of the high-j valence-nucleon vectors, see Fig. 1. The angular momentum vector of the valence neutrons, j_ν, is aligned with the rotation axis, whereas the angular momentum vectors of the proton holes, j_{π_1} and j_{π_2}, are oriented along the symmetry axis at an angle θ to it. The angle between the angular momentum vectors of the proton holes, j_{π_1} and j_{π_2}, is 2θ. R is the core contribution to the total angular momentum, as shown in Fig. 1. The total spin is generated by the closing of the two shears toward the rotation axis and is given as

$$I = j_\nu + (j_{\pi_1} + j_{\pi_2})\cos\theta + \Im\omega_{sh}. \tag{1}$$

The term $\Im\omega_{sh}$ describes the coupling between the shears mechanism and collective rotation. Here, $\Im$ denotes the rotational moment of inertia, and ω_{sh} denotes

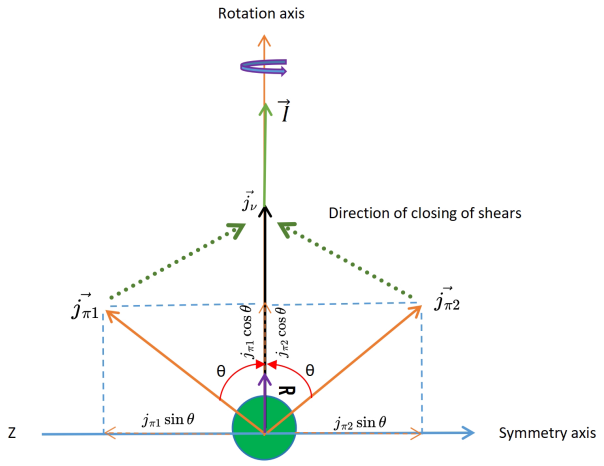


Fig. 1. (color online) Schematic diagram illustrating the coupling of the angular-momentum vectors of the proton-hole and neutron-particle configurations in antimagnetic rotation to generate the total spin/angular momentum.

the rotational frequency, given as

$$\omega_{sh} = \frac{1.5V_{\pi\nu}\cos\theta}{j_{\rm eff}} - \frac{6V_{\pi\pi}\cos 2\theta\cos\theta}{n j_{\rm eff}}, \tag{2}$$

where $V_{\pi\nu}$ and $V_{\pi\pi}$ are the proton-neutron and proton-proton interaction strengths, respectively, n is the product of the number of valence neutrons and proton holes, and $j_{\rm eff}$ is the effective blade length of the two proton holes, given by $j_{\rm eff} = (j_{\pi_1} + j_{\pi_2})/2$. For example, for two $g_{9/2}$ proton holes in a given configuration, the Pauli exclusion principle prevents both holes from occupying the same magnetic substate. Therefore, the maximum aligned configuration corresponds to $m_j = 9/2$ and $7/2$, giving $j_{\pi_1} = 9/2$ and $j_{\pi_2} = 7/2$. Consequently, $j_{\rm eff} = (9/2+7/2)/2 = 4\hbar$. The first two terms of Eq. (1) are represented by I_{sh}, the total angular momentum, or spin, produced by the twin shear mechanism. Thus, Eq. (1) can be expressed as

$$I = I_{sh} + \Im\omega_{sh}. \tag{3}$$

For each experimentally observed spin state, the corresponding shears angle θ is obtained by solving Eq. (3) for the adopted configuration of proton holes and neutron particles. The angular momentum vectors of the proton holes and neutron particles are fixed by the chosen configuration, whereas the experimental spin I is used as input to determine the corresponding shears angle θ. The obtained value of θ is then used to determine the rotational frequency through Eq. (5) and the excitation energies through the recursive relation described below. The collective moment of inertia $\Im$ is determined from the equation

$$\Im\omega_{sh}|_{(\theta=0^0)} = I_{\max} - I_{sh}^{\max}, \tag{4}$$

where $I_{\max}$ is the highest observed spin and $I_{sh}^{\max}$ is the maximum spin generated through the shears mechanism. Generally, the core rotational contribution in AMR bands is small; however, when the intrinsic shears angular momentum alone does not reproduce the observed bandhead spin, a small constant core contribution is included to account for the collective rotation of the core. The magnitude of $\Im$ determines the extent of coupling between collective rotation and the shears mechanism in generating the total spin. The total rotational frequency arising from the coupling of the core $\omega_{cr}(I)$ and shears $\omega_{sh}(I)$ frequencies is

$$\omega(I) = \omega_{cr}(I) - \omega_{sh}(I), \tag{5}$$

where the core rotational frequency is $\omega_{cr}(I) = (2I+1)/2\Im_{cr}$, and the core moment of inertia, $\Im_{cr}$, is extracted from the slope of the spin-versus-frequency plot before the first neutron alignment with the rotational axis. The experimental $\omega(I)$ for a given excitation energy E_γ is calculated as

$$\omega(I) \approx \frac{E_\gamma}{\sqrt{(I+\frac{3}{2})^2 - K^2} - \sqrt{(I-\frac{1}{2})^2 - K^2}}, \tag{6}$$

where K is the spin value of the lowest-energy state. For a given shears angle θ, the reduced quadrupole transition probability is given by

$$B(E2) = \frac{15}{32\pi}(eQ_{\rm eff})^2 \sin^4\theta, \tag{7}$$

where $(eQ_{\rm eff})$ is the effective quadrupole moment, as reported in Refs. [4, 17, 30]. Here, $(eQ_{\rm eff}) \approx 1.2$ eb, which is consistent with the value obtained in the $A \approx 100-110$ mass region. The dynamic moment of inertia $\Im^{(2)}$ is determined from the experimental E_γ values using the available partial level scheme, as follows:

$$\Im^{(2)} = \frac{4}{E_\gamma(I+2\rightarrow I) - E_\gamma(I\rightarrow I-2)}, \tag{8}$$

where I denotes the spin of the intermediate level.

III. CALCULATION AND DISCUSSION OF RESULTS

The calculations presented in this section have been carried out using the semiclassical particle-rotor model to investigate the possible existence of an antimagnetic rotation structure in the $\nu h_{11/2}$ negative-parity bands of ^{107,109,111}Pd. The adopted parameters and configurations of proton holes and neutron particles are chosen to reproduce the experimentally observed spin, parity, and high-spin range of each band within the framework of the shears mechanism. This is further assessed by comparing the calculated $E(I)$ *vs* $I(I+1)$, $I-\hbar\omega$, $B(E2)$, and $\Im^{(2)}/B(E2)$ systematics with the available experimental data, and the configuration that provides the most consistent overall description is adopted. For each adopted configuration, the quantities j_ν, j_{π_1}, j_{π_2}, n, $I_{sh}^{\max}$, and the collective moment of inertia are fixed by the chosen configuration. The collective core moment of inertia, $\Im_{cr}$, is obtained from the slope of the experimental spin versus $\hbar\omega$ plot at lower spins before the first alignment of the shears. The proton-neutron interaction strength is fixed at $V_{\pi\nu} = 1.2$ MeV, following earlier SCM studies of the Pd and Cd isotopes [6, 8, 10, 19, 27, 28], while $V_{\pi\pi}$ is varied within the accepted range of 0.15−0.20 MeV.

The shears angle θ is the dynamical variable of the SCM and varies from 90° to 0° for a fixed configuration, producing an increase in spin through Eqs. (1)−(3). Simultaneously, the reduced transition probability decreases according to the $\sin^4\theta$ dependence of Eq. (7). Thus, the evolution of both the spin I and the calculated $B(E2)$ values is governed by the geometrical closing of the shears blades.

Figure 2 shows the energy-level scheme of the negative-parity bands of ^{107,109,111}Pd, redrawn from Refs. [52, 53]. These experimentally established level sequences provide the basis for the present semiclassical particle-rotor model investigation of a possible antimagnetic rotation structure in these nuclei. The observed band structures, excitation energies, spin assignments, and γ-ray transition energies are used to extract the rotational frequencies and determine the proton-hole and neutron-particle configurations suitable for reproducing the exper-

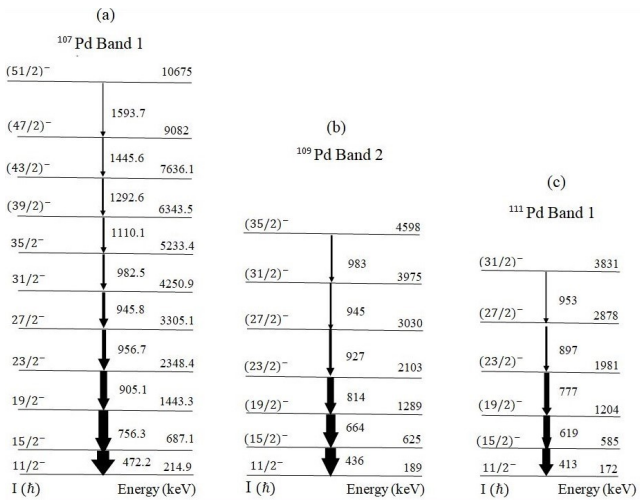


Fig. 2. The partial level schemes of ^{107,109,111}Pd show the negative-parity bands, with γ-ray and level energies given in keV, redrawn from Refs. [52, 53].

imental spin values within the shears mechanism. The experimentally observed maximum spins in these bands also provide an important constraint on estimating the contributions of the shears mechanism and core rotation to the total angular momentum generation. All three negative-parity bands are built on the $I^{\pi} = 11/2^{-}$ level at excitation energies of 214.9, 189, and 172 keV, respectively.

The occupation of the valence proton-hole and neutron-particle orbitals depends on the spin, parity, and spin range of the observed bands that can be generated within the framework of the shears mechanism. Therefore, the configurations of proton holes and neutron particles for ^{107}Pd, ^{109}Pd, and ^{111}Pd are $\pi(g_{9/2})^{-4}\otimes\nu(h_{11/2})^{3}$, $\pi(g_{9/2})^{-2}\otimes\nu[h_{11/2}(d_{5/2})^{2}]$, and $\pi(g_{9/2})^{-2}\otimes\nu(h_{11/2})+2\hbar$, respectively. The negative-parity bands of these three isotopes exhibit similar experimental characteristics; however, different configurations of proton holes and neutron particles are required because they terminate at different spins, namely $(51/2)^{-}$, $(35/2)^{-}$, and $(31/2)^{-}$, respectively.

Figure 3 compares the experimental and SCM-calculated excitation energies as a function of $I(I+1)$ for the negative-parity bands of ^{107,109,111}Pd. The excitation energy of the state with spin I is calculated using $E(I) = E(I-2)+\hbar\omega(I)+\hbar\omega(I-2)$, where ω is given by Eq. 5. The recursive calculation is initiated using the experimental excitation energy of the spin state corresponding to the SCM bandhead. For example, for ^{107}Pd, the SCM bandhead is the $27/2^{-}$ state. Therefore, the recursive calculation is initiated using the experimental excitation energy of the $27/2^{-}$ state, $E(27/2^{-}) = 3.3051$ MeV. It is clear from the figure that the calculated excitation energies closely reproduce the experimental data over the observed spin range, indicating that the adopted configurations provide a satisfactory description of the rotational spectra.

Both the experimental and calculated excitation energies exhibit an approximately linear dependence on $I(I+1)$, consistent with the rotational energy relation $E(I) \propto I(I+1)$ and thereby confirming the rotational character of these bands. The straight dotted line represents the linear fit to the experimental excitation energies of the lower-spin states for comparison. Small deviations from perfect linearity become visible at higher spins, which may be associated with the progressive alignment of high-j proton holes and neutron particles responsible for the antimagnetic rotational bands. Such deviations may also reflect the onset of non-collective rotation and rotational-frequency-dependent shape evolution, as commonly observed in transitional nuclei in the A≈110 mass region. A gradual decrease in the slope of the curves with increasing spin suggests an increase in the nuclear moment of inertia, consistent with the progressive alignment of high-j proton holes and neutron particles responsible for the antimagnetic rotational bands.

Figure 4 compares the variation of the experimental spin with $\hbar\omega$ for the negative-parity bands of ^{107,109,111}Pd with the calculated results for configurations (i) $\pi(g_{9/2})^{-2}\otimes\nu(h_{11/2})^{3}$ and $\pi(g_{9/2})^{-4}\otimes\nu(h_{11/2})^{3}$ for ^{107}Pd, (ii) $\pi(g_{9/2})^{-2}\otimes\nu(h_{11/2},(d_{5/2})^{2})$ for ^{109}Pd, and (iii) $\pi(g_{9/2})^{-2}\otimes\nu(h_{11/2})^{1}+2\hbar$ for ^{111}Pd using SCM. Among the various possible configurations examined, the adopted ones provide the best overall agreement with the experimental $I-\hbar\omega$ relation while reproducing the observed spin, parity, and spin range. Following the standard SCM prescription, the proton-proton interaction strength $V_{\pi\pi}$ is varied within the range 0.15−0.20 MeV, and the value that yields the minimum RMS deviation between the calculated and experi-

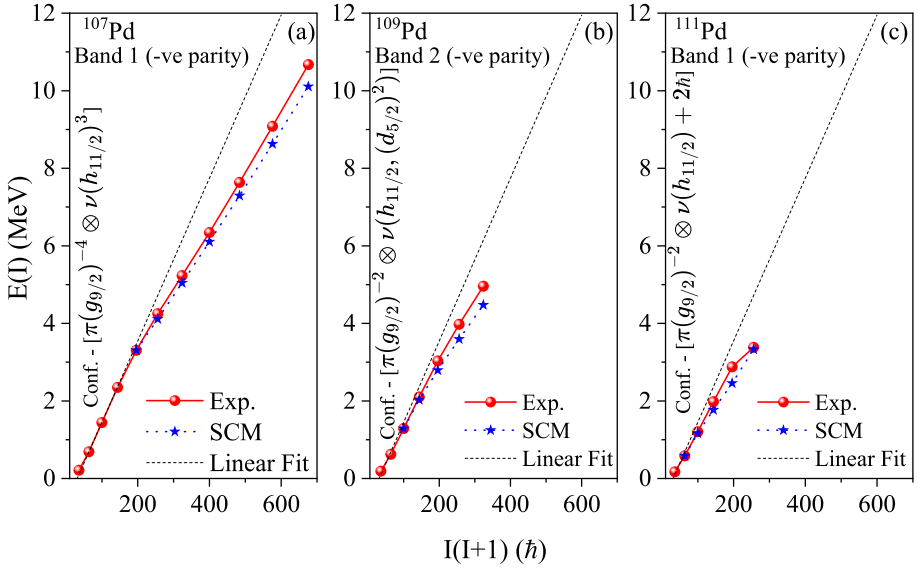


Fig. 3. (color online) Experimental and SCM-calculated excitation energies, $E(I)$ (in MeV), as a function of $I(I+1)$ for the negative-parity bands of ^{107,109,111}Pd [52, 53]. The dotted line indicates the linear fit to the experimental data at low spins.

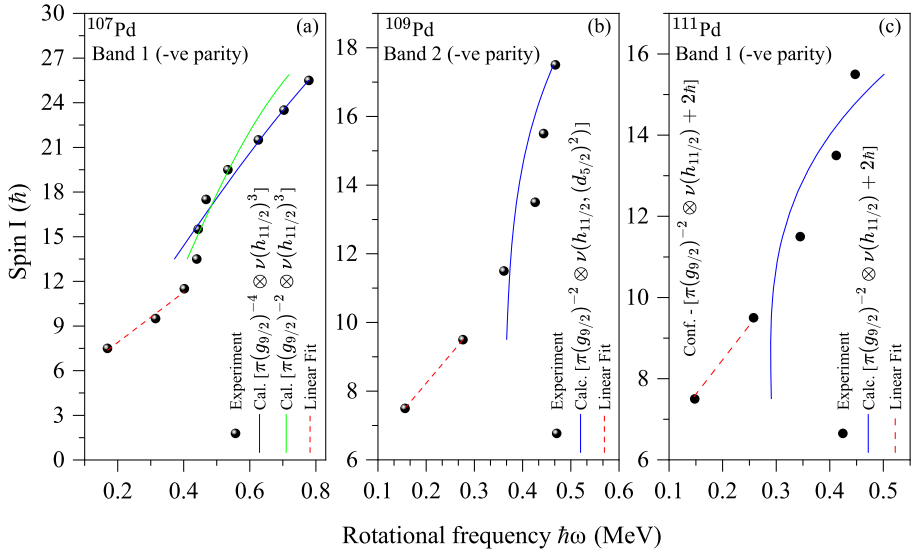


Fig. 4. (color online) The variation of the spin I ($\hbar$) with $\hbar\omega$ (MeV) for ^{107,109,111}Pd. The solid spheres represent the experimental values, and the line corresponds to the values calculated using SCM. The dashed red line represents the linear fit to the experimental spin plot before the onset of the shear-closing mechanism.

mental $I-\hbar\omega$ values is adopted. The resulting RMS deviations are 0.030, 0.046, and 0.073 for ^{107}Pd, ^{109}Pd, and ^{111}Pd, respectively. The shears parameters used for the configuration $\pi(g_{9/2})^{-4}\otimes\nu(h_{11/2})^3$ of ^{107}Pd are $j(=j_{\rm eff})=6\,\hbar$, $j_\nu=27/2\,\hbar$, $V_{\pi\nu}=1.2$ MeV, $V_{\pi\pi}=0.2$ MeV, $n=12$; where n is the number of proton-hole and neutron-particle pairs. The maximum spin within the shears mechanism for this configuration is $I_{sh}^{\rm max}=51/2\,\hbar$. The maximum spin in the partial level scheme is $I_{\rm max}=51/2\,\hbar$, see Fig. 2 (a). Therefore, the core contribution to the spin, and hence the core moment of inertia, is zero ($\Im=0\,\hbar^2{\rm MeV}^{-1}$). The neutron contribution to the total spin, also known as the AMR band head, is $I=27/2\,\hbar$, and the corresponding $\omega(I)=0.433$ MeV. The core contribution to the moment of inertia, $\Im_{cr}\approx 17.4\,\hbar^2{\rm MeV}^{-1}$, is obtained from the slope of the least-squares fit curve to the spin I ($\hbar$) *vs* $\hbar\omega$ (MeV) values from the partial level scheme of Fig. 2 (a) before the alignment of the spins of the neutron particles along the axis of rotation. It is clear from the figure that the calculated spin I for the configuration $\pi(g_{9/2})^{-4}\otimes\nu(h_{11/2})^3$ reproduces the experimental spin values for the corresponding experimental ω values in the spin range $(31/2-51/2)\,\hbar$. It should be noted that if the configuration $\pi(g_{9/2})^{-2}\otimes\nu(h_{11/2})^3$ is considered, the calculated $I-\omega$ relation does not agree well with the experimental results for $I\geqslant 47/2\,\hbar$, see the green line in Fig. 4 (a). Thus, the configuration $\pi(g_{9/2})^{-4}\otimes\nu(h_{11/2})^3$ provides a satisfactory description of the observed AMR behavior in ^{107}Pd.

Figure 4 (b) is for ^{109}Pd, where the configuration suitable for the AMR study is $\pi(g_{9/2})^{-2}\otimes\nu[h_{11/2}(d_{5/2})^2]$, which gives a maximum contribution to the spin of $I=35/2\,\hbar$. In this case, the contribution from the neutron particles is $I_{\rm min}=19/2\,\hbar$, and the maximum spin within the shears mechanism is $I_{sh}^{\rm max}=35/2\,\hbar$; the experimental maximum spin is also $I_{\rm max}=35/2\,\hbar$. Therefore, the core contribution to the spin is zero, and the corresponding moment of inertia is $\Im=0\,\hbar^2{\rm MeV}^{-1}$. The shears parameters are $j=4\,\hbar$, $j_\nu=19/2\,\hbar$, $V_{\pi\nu}=1.2$ MeV, $V_{\pi\pi}=0.15$ MeV, $n=6$. The AMR band-head frequency is $\hbar\omega\approx 0.27$ MeV for $I=19/2\,\hbar$. The value $\Im_{cr}\approx 15.4\,\hbar^2{\rm MeV}^{-1}$ is obtained from the slope of the least-squares fit curve to the spin I ($\hbar$) *vs* $\hbar\omega$ (MeV) values from the partial level scheme of Fig. 2 (b) before the alignment of the spins of the neutron particles along the axis of rotation. The shears mechanism reproduces the experimental spin range $(23/2-35/2)\,\hbar$.

Figure 4 (c) is for the ^{111}Pd nucleus with the proton-hole and neutron-particle configuration $\pi(g_{9/2})^{-2}\otimes\nu(h_{11/2})+2\hbar$. Here, the configuration $\pi(g_{9/2})^{-2}\otimes\nu(h_{11/2})$ yields a maximum angular momentum of $27/2\,\hbar$, which is $2\hbar$ lower than the maximum experimental angular momentum of $31/2\,\hbar$. Therefore, a constant $2\hbar$ core contribution, which accounts for the small collective rotation of the core at the onset of the band, is included. The shears parameters are $j=4\,\hbar$, $j_\nu=15/2(=11/2+2)\,\hbar$, $V_{\pi\nu}=1.2$ MeV, $V_{\pi\pi}=0.15$ MeV, $n=2$. The maximum shears contribution to the spin is $I_{sh}^{\rm max}=31/2\,\hbar$, the experimental maximum spin is $I_{\rm max}=31/2\,\hbar$, and hence $\Im=0\,\hbar^2{\rm MeV}^{-1}$. The AMR band-head frequency is $\hbar\omega\approx 0.25$ MeV for $I=15/2\,\hbar$. The value $\Im_{cr}\approx 14.6\,\hbar^2{\rm MeV}^{-1}$ is obtained from the slope of the least-squares fit curve to the spin I ($\hbar$) *vs* $\hbar\omega$ (MeV) values from the partial level scheme of Fig. 2 (c) before the alignment of the spins of the neutron particles along the axis of rotation. This configuration successfully reproduces the experimental spin in the range $(23/2-31/2)\,\hbar$.

Figure 5 shows the variation of the shears angle θ with spin and rotational frequency for the negative-parity bands of ^{107,109,111}Pd. The shears angle decreases with increasing spin, demonstrating the progressive closing of the proton-hole shears blades toward the neutron-particle angular momentum vector, which is characteristic of the shears-closing mechanism in antimagnetic rotation. Figures 5(a)–(c) show the variation of θ with spin, while Figs. 5(a′)–(c′) show the corresponding variation with rotational frequency $\hbar\omega$, reflecting the same geometrical evolution of the shears mechanism.

Figure 6(a) shows the variation in the calculated reduced transition probability $B(E2)$ as a function of $\hbar\omega$ for the ^{107,109,111}Pd nuclei within the SCM framework, since

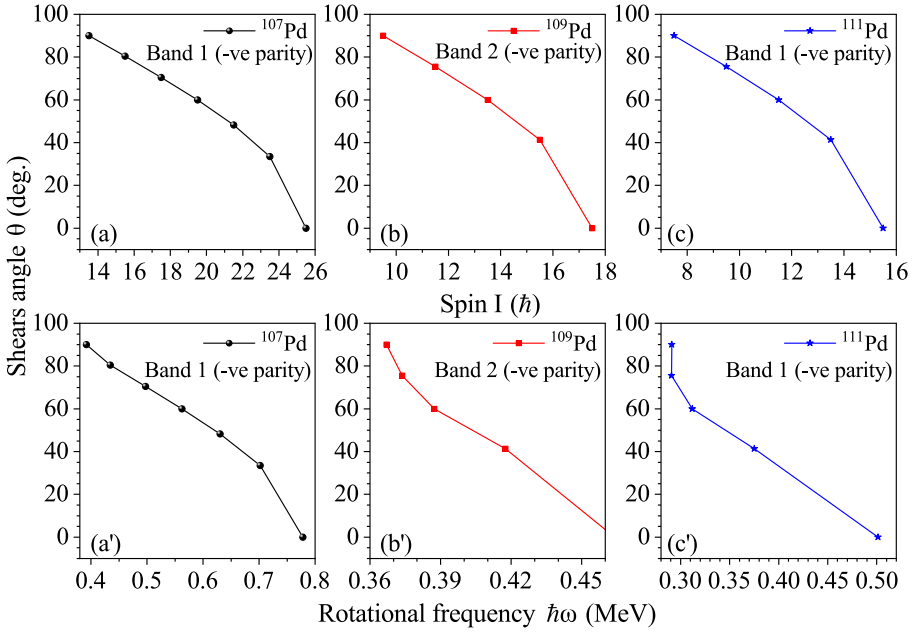


Fig. 5. (color online) The variation of the shears angle, θ, as a function of spin, I, for the negative-parity bands of ^{107,109,111}Pd is shown in panels (a), (b), and (c), respectively. Panels (a′), (b′), and (c′) show the corresponding variation of θ as a function of the rotational frequency, $\hbar\omega$.

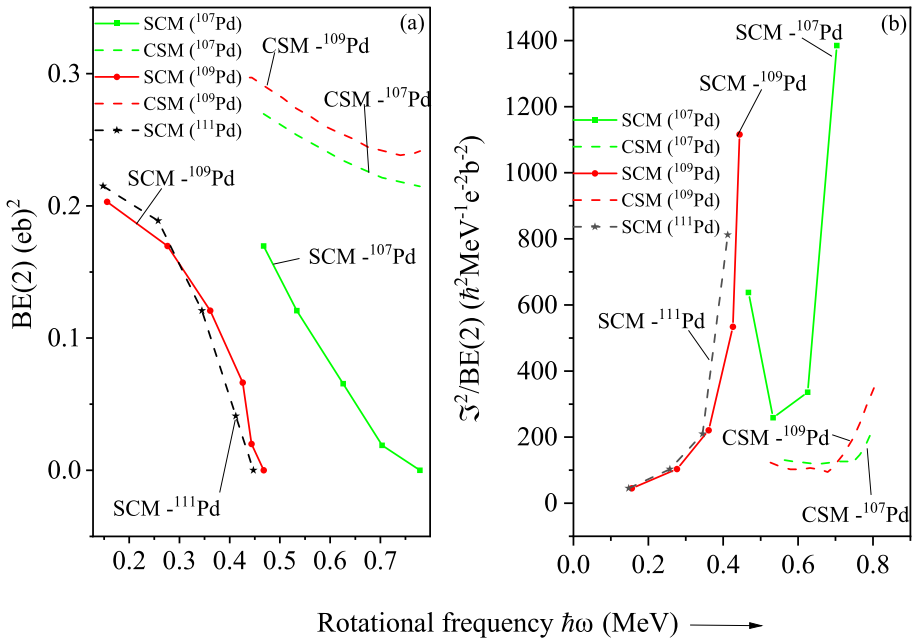


Fig. 6. (color online) The calculated reduced transition probability $B(E2)$ and $\Im^{(2)}/B(E2)$ as functions of $\hbar\omega$ (MeV) for the ^{107,109,111}Pd nuclei. The dotted line corresponds to the CSM calculations reported in Ref. [49].

lifetime measurements are not available for these nuclei. It reflects the evolution of quadrupole collectivity with the closing of the shears blades. The decrease in the calculated $B(E2)$ values originates from the closing of the shears blades, *i.e.*, the reduction of the shears angle shown in Fig. 5, consistent with the $\sin^4\theta$ dependence of Eq. (7). The decreasing trend of the $B(E2)$ values with increasing $\hbar\omega$, together with their magnitude remaining below 0.21 $(eb)^2$ throughout the entire $\hbar\omega$ range, is consistent with the literature [54] and is a signature of the AMR structure at high spin. The CSM predictions (dotted lines) for the $B(E2)$ values of the ^{107,109}Pd nuclei also show a decreasing trend with increasing $\hbar\omega$, although the magnitudes of the two calculations differ.

Figure 6(b) shows the variation of the ratio $\mathfrak{I}^{(2)}/B(E2)$ with $\hbar\omega$ for the ^{107,109,111}Pd nuclei calculated within the SCM framework, together with the corresponding CSM results for ^{107,109}Pd. The increasing trend of $\mathfrak{I}^{(2)}/B(E2)$ further supports the AMR character of these nuclei.

The present SCM analysis provides a consistent description of the rotational properties of the negative-parity bands in ^{107,109,111}Pd and suggests that the observed high-spin structures exhibit the characteristic features associated with antimagnetic rotation.

IV. CONCLUSIONS

The negative-parity bands of ^{107,109,111}Pd have been investigated for the possible presence of an AMR structure within the framework of the semiclassical particle-rotor model. The experimentally observed spin–frequency behavior is reasonably reproduced using suitable proton-hole and neutron-particle configurations: $\pi(g_{9/2})^{-4}\otimes\nu(h_{11/2})^3$, $\pi(g_{9/2})^{-2}\otimes\nu[h_{11/2}(d_{5/2})^2]$, and $\pi(g_{9/2})^{-2}\otimes\nu(h_{11/2})+2\hbar$, respectively, for the ^{107,109,111}Pd isotopes. The decreasing trend of the calculated $B(E2)$ values and the increasing trend of the ratio $\mathfrak{I}^{(2)}/B(E2)$ with $\hbar\omega$ indicate the presence of an AMR structure in the negative-parity bands of the ^{107,109,111}Pd nuclei. The calculated decrease in the shears angle with increasing spin further confirms the characteristic shears-closing mechanism associated with antimagnetic rotation. However, lifetime measurements for these nuclei are required to confirm the present predictions.

References

[1] S. Frauendorf, Nucl. Phys. A **557**, 259 (1993)
[2] S. Frauendorf, J. Meng, J. Reif, in *Proc. Conf. Physics from Large Gamma-Ray Detector Arrays, Berkeley, Vol.* **II**(Berkeley: Lawrence Berkeley National Laboratory, 1994), p. 52
[3] S. Frauendorf, Rev. Mod. Phys. **73**, 463 (2001)
[4] R. M. Clark, A. O. Macchiavelli, Annu. Rev. Nucl. Part. Sci. **50**, 1 (2000)
[5] S. Zhu, U. Garg, A. V. Afanasjev *et al.*, Phys. Rev. C **64**, 041302 (2001)
[6] S. Sihotra, D. Kumar, M. Kaur *et al.*, Phys. Rev. C **102**, 034321 (2020)
[7] M. Sugawara, H. Kusakari, T. Morikawa *et al.*, Phys. Rev. C **92**, 024309 (2015)
[8] V. Singh, S. Sihotra, S. Roy *et al.*, J. Phys. G: Nucl. Part. Phys. **44**, 075105 (2017)
[9] A. Sharma, R. Raut, S. Muralithar *et al.*, Phys. Rev. C **103**, 024324 (2021)
[10] N. Rather, S. Roy, P. Datta *et al.*, Phys. Rev. C **89**, 061303(R) (2014)
[11] C. Majumder, H. P. Sharma, S. Chakraborty *et al.*, J. Phys. G: Nucl. Part. Phys. **47**, 125104 (2020)
[12] N. Rather, P. Datta, S. Chattopadhyay *et al.*, Proceedings of the DAE Symp. on Nucl. Phys. **59**, 108 (2014)
[13] D. Choudhury, A. K. Jain, M. Patial *et al.*, Phys. Rev. C **82**, 061308(R) (2010)
[14] A. J. Simons, R. Wadsworth, D. G. Jenkins *et al.*, Phys. Rev. Lett. **91**, 162501 (2003)
[15] A. J. Simons, R. Wadsworth, D. G. Jenkins *et al.*, Phys. Rev. C **72**, 024318 (2005)
[16] D. Choudhury, A. K. Jain, G. A. Kumar *et al.*, Phys. Rev. C **87**, 034304 (2013)
[17] P. Datta, S. Chattopadhyay, S. Bhattacharya *et al.*, Phys. Rev. C **71**, 041305(R) (2005)
[18] C. J. Chiara, S. J. Asztalos, B. Busse *et al.*, Phys. Rev. C **61**, 034318 (2000)
[19] S. Roy, S. Chattopadhyaya, P. Datta *et al.*, Phys. Lett. B **694**, 322 (2011)
[20] C. J. Chiara, D. B. Fossan, V. P. Janzen *et al.*, Phys. Rev. C **64**, 054314 (2001)
[21] S. Ali, S. Rajbanshi, B. Das *et al.*, Phys. Rev. C **96**, 021304 (2017)
[22] S. Rajbanshi, S. Roy, S. Nag *et al.*, Phys. Lett. B **748**, 387 (2015)
[23] P. W. Zhao, J. Peng, H. Z. Liang *et al.*, Phys. Rev. Lett. **107**, 122501 (2011)
[24] S. Roy and S. Chattopadhyay, Phys. Rev. C **87**, 059801 (2013)
[25] C. Majumdar, S. Chakraborty, S. S. Tiwary *et al.*, Proceedings of the DAE Symp. on Nucl. Phys. **60**, 294 (2015)
[26] C. Majumder, H. P. Sharma, S. Chakraborty and S. S. Tiwary, Int. J. Mod. Phys. E **27**, 4 (2018)
[27] S. Sihotra, Int. J. Mod. Phys. E **31**, 2250020 (2022)
[28] Y. K. Pan, K. Y. Ma, J. B. Lu, Chin. Phys. C. **46**, 094001 (2022)
[29] S. Chakraborty, H. P. Sharma, S. S. Tiwary *et al.*, J. Phys. G: Nucl. Part. Phys. **47**, 015103 (2020)
[30] P. Chauhan, S. Sihotra, R. Joshi *et al.*, Nucl. Phys. A **1055**, 123016 (2025)
[31] P. Chauhan, S. Sihotra, R. Joshi *et al.*, Int. J. Mod. Phys. E **33**, 2450042 (2024)
[32] C. Majumder, H. P. Sharma, S. S. Tiwary *et al.*, Braz. J. Phys **49**, 539 (2019)
[33] C. M. Petrachea, P.M. Walker, S. Guo *et al.*, Phys. Lett. B **795**, 241 (2019)

[34] S. Guo, C. M. Petrache, D. Mengoni *et al*., Phys. Rev. C **102**, 044320 (2020)
[35] J. Peng, Int. J. Mod. Phys. E **26**, 1750051 (2017)
[36] J. Lin, Y. K. Wang, C. Xu *et al*., Phys. Rev. C **107**, 014307 (2023)
[37] H. Jia, B. Qi, C. Liu *et al*., Phys. Rev. C **97**, 024335 (2018)
[38] P. Zhang, B. Qi, S. Y. Wang, Phys. Rev. C **89**, 047302 (2014)
[39] W. J. Sun, H. D. Xu, J. Li *et al*., Chin. Phys. C. **40**, 084101 (2016)
[40] M. Wang, W. J. Sun, B. H. Sun *et al*., Eur. Phys. J. A **56**, 31 (2020)
[41] X. W. Li, J. Li, J. B. Lu *et al*., Phys. Rev. C **86**, 057305 (2012)
[42] K. Y. Ma, J. B. Lu, J. Li *et al*., Phys. Rev. C. **100**, 014326 (2019)
[43] C. M. Petrache, S. Frauendorf, B. F. Lv *et al*., Phys. Rev. C **99**, 041301(R) (2019)
[44] C. M. Petrache, S. Frauendorf, M. Matsuzaki *et al*., Phys. Rev. C **86**, 044321 (2012)
[45] H. Jia and B. Qi, Phys. Rev. C. **110**, 044303 (2024)
[46] E. S. Paul, C. W. Beausang, R. M. Clark *et al*., J. Phys. G: Nucl. Part. Phys. **20**, 1405 (1994)
[47] J. Q. Ma, Z. H. Zhang, Nucl. Phys. A **1016**, 122319 (2021)
[48] Z. H. Zhang, Phys. Rev. C **99**, 029901 (2019)
[49] Z. Qiao, Y. C. Hao, H. Wang *et al*., Phys. Rev. C **112**, 044315 (2025)
[50] Z. H. Zhang, Chin. Phys. C **43**, 054107 (2019)
[51] Z. H. Zhang, P. W. Zhao, J. Meng *et al*., Phys. Rev. C **87**, 054314 (2013)
[52] K. R. Pohl, P. H. Regan, J. E. Bush *et al*., Phys. Rev. C **53** 2682(1996)
[53] E. A. Stefanova, S. Lalkovski, A. Korichi *et al*., Phys. Rev. C **86**, 044302 (2012)
[54] S. Kumar, S. Singh, B. Singh *et al*., At. Data Nucl. Data Tables **165**, 101735 (2025)